PAPER

Mode II adhesion energy analysis of stiction-failed poly-Si #cantilevers using a MEMS load cell

To cite this article: Behnam Kheyraddini Mousavi et al 2019 J. Micromech. Microeng. 29 075013

View the article online for updates and enhancements.



IOP ebooks™

Bringing together innovative digital publishing with leading authors from the global scientific community.

Start exploring the collection-download the first chapter of every title for free.

Mode II adhesion energy analysis of stiction-failed poly-Si μ cantilevers using a MEMS load cell

Behnam Kheyraddini Mousavi¹, Arash Kheyraddini Mousavi^{2,5}, Tyler Jordan Hieber³, James Chen⁴ and Zayd Chad Leseman³

- ¹ Department of ElectroMechanical Engineering, Northern New Mexico College, Espanola, NM, United States of America
- ² Mechanical Engineering Department, New Mexico Institute of Mining and Technology, Socorro, NM, United States of America
- ³ Department of Mechanical and Nuclear Engineering, Kansas State University, Manhattan, KS, United States of America
- ⁴ Department of Mechanical and Aerospace Engineering, University of Buffalo, Bufallo, NY, United States of America

E-mail: arash.mousavi@nmt.edu

Received 18 January 2019, revised 25 March 2019 Accepted for publication 8 April 2019 Published 31 May 2019



Abstract

This paper studies the Mode II adhesion energy of a Poly-Si μ cantilever stiction failed on a poly-Si substrate. A custom flexural microelectromechanical systems (MEMS) load cell and an interferometer are used to measure the applied forces and measure the deflections in real time. From this data the Mode II strain energy release rates were determined to range between 0.520–5.10 mJ m⁻².

Keywords: MEMS, stiction failure, critical strain energy release rate, adhesion energy, Mode II

(Some figures may appear in colour only in the online journal)

1. Introduction

With continued research and development microelectromechanical systems (MEMS) are finding their way into many commercial applications. The applications cover a wide range from modern electronics [1–4] to optoelectronics [3, 4] and mechanical systems such as sensors [5, 6] and actuators [7]. Some common examples include carbon nanotubes, carbon nanofibers [8], nanostructured anti-reflection coatings [4], phononic crystals [6, 9], micromirror arrays [10], and MEMS gyroscopes [5].

Though many types of MEMS have been made commercially available, to date there are still no MEMS which contain moving parts that have rubbing surfaces. In an article by Romig *et al* [11, 12], a taxonomy for MEMS devices was developed that is based on motion and contact. In this taxonomy MEMS

were broken into four classifications. Class I devices contain no moving parts, such as strain gauges or inkjet printheads [13]. Class II MEMS have moving parts but no (intentional) contact between surfaces such as gyros, comb drive actuators, and resonators. Class III MEMS have moving parts and impacting surfaces such as Texas Instrument's DMD, micro-relays, valves, and pumps. Class IV MEMS devices have moving parts and impacting and rubbing surfaces. Class IV MEMS are not commercially available due to issues they encounter with adhesion [14, 15], friction [16] and wear. Because of the length scale on which MEMS and NEMS exist surface forces dominate even over gravitational forces [17]. An example of this is stiction failure. Stiction describes the (semi)-permanent failure of a MEMS device on its substrate. A common reason for stiction failure is the high surface tension forces induced by liquids trapped between the device its substrate (usually as a result of condensation). These issues impair the reliability of the device and make their mass production less attractive to manufacturers.

⁵ Author to whom any correspondence should be addressed.

To mitigate adhesion, friction and wear in MEMS researchers have reverted to use of lubricants such as OTS [18–21], DDMS [21, 22] and octadecene [23, 24]. These lubricants are monolayers of material on the surfaces of the devices. Though chemically bonded to the substrate these coatings eventually wear off and do not completely avoid wear. These choices of lubricants differ from common lubricants for macroscopic systems because MEMS are commonly made from Si, an uncommon structural material at the macroscale.

A considerable amount of effort has gone into determining the critical strain enery release rate (adhesion energy), G, of MEMS with Mode I type failures. De Boer $et\ al\ [25]$ developed a model to determine G by using s-shaped failures of μ cantilever beams. This method has been employed by many others [14, 26–29]. A more exact method for determination of G using the same method, but including nonlinear effects was published more recently [14]. Though Mode I is fairly well understood Mode II has been neglected.

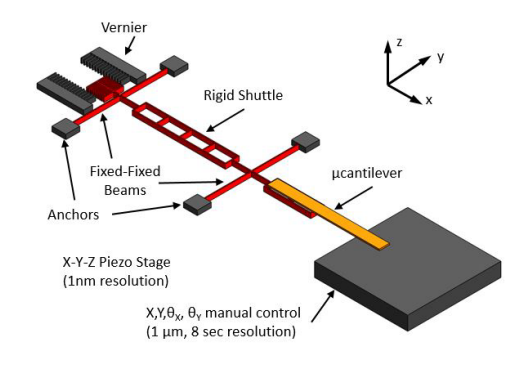
Herein a technique to determine the Mode II contribution of a poly-Si μ cantilever on a poly-Si surface is developed. Controlled stick-slip events are induced by instrumenting one of the surfaces with a force sensor such that the adhesion energy between the surfaces can be determined. In this work, the surfaces are both dry in that there is no lubricant between the surfaces.

2. Experimental design & setup

2.1. The MEMS force sensor

The MEMS device used here is illustrated in figure 1(a). The device is composed of a floating rigid shuttle connected to its native substrate through four compliant arms. It is also equipped with a vernier which can be used to measure the relative motion of the shuttle with respect to the substrate with $100\,\mathrm{nm}$ resolution. The flexural arms are more than $10\,000$ times more compliant than the shuttle and can be considered as two fixed-fixed beam springs. Due to the parallel configuration the deflection in each arm is equal to the displacement of the shuttle and its transverse force contributes to $\frac{1}{4}$ of the total reaction force acting on the shuttle. This force can be accurately determined once the shuttle deflection is measured using the vernier, figure 1(a).

The fabrication process used to make the MEMS actuator is detailed in [7] and [30]. The following is a brief discussion of the process. A (100) silicon on insulator (SOI) wafer with 20 μ m thick device-layer, 1 μ m buried oxide (BOX) and 600 μ m handle layer was utilized. The device and the handle layers are both p-type doped with boron. A single mask process was used to transfer the pattern to the photoresist (PR). The device layer was then etched to the BOX layer by deep reactive ion etching [31]. This anisotropic process creates high aspect ratio structures with nearly vertical sidewalls. The PR layer is finally removed using acetone, isopropyl alcohol, and deionized (DI) water rinses. Oxygen plasma is then used to remove any small remaining amount of PR on the Si surface. Finally, the actuator is released by etching the BOX layer in an HF bath and rinsed in DI water.



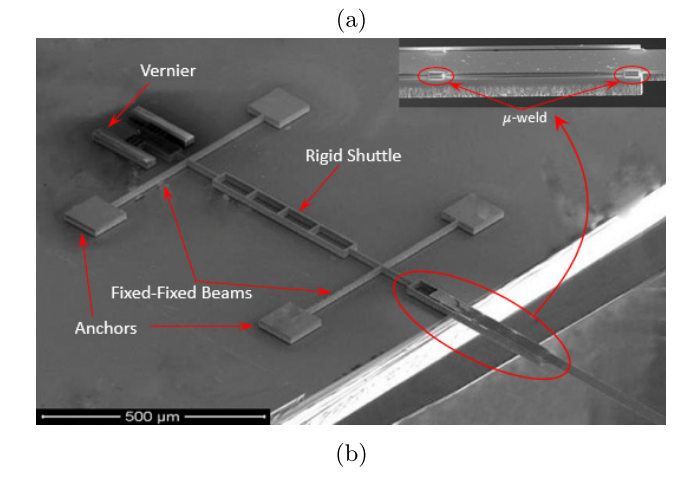


Figure 1. (a) Schematic representation of Mode II experimental setup. The force measurement MEMS device is represented by the rigid shuttle, four flexural arms and a vernier. The μ cantilever specimen is welded on its left end and stiction failed on the substrate fixed on the piezo stage on its right. (b) SEM micrograph of the setup. Note that the μ cantilever extends beyond the edge of the image for almost another 700 μ m.

The μ cantilever beam specimen and the substrate it was failed on was fabricated at Sandia National Laboratories using the Sandia Ultra-planar, Multi-level MEMS Technology 5 (SUMMiT VTM). This process uses a specific set of fabrication processes to make MEMS devices by surface micromachining using as many as 15 masks [32, 33]. These are the same materials that were used in the experiments in the following [14, 25, 29] and therefore the results in this paper are directly comparable. The specific μ cantilever beam used was 30 μ m wide and 1500 μ m long.

2.2. Experimental procedure

2.2.1. Procedure for controlled stiction failure. In these experiments the bottom surface of the protruding μ cantilever is stiction failed on the substrate then peeled off along its length in a step wise manner. The peeling force is generated by the piezo stage, on which the MEMS sensor is mounted, and transmitted to the μ cantilever by the MEMS sensor. Before the beam can be adhered to the substrate, it must be aligned. This is accomplished using a manual XY stage and two goniometers on which the substrate is mounted. The position is adjusted so that no more than 155 μ m of the μ cantilever is overlapped. A drop of DI water is used to wet the interface. As the water

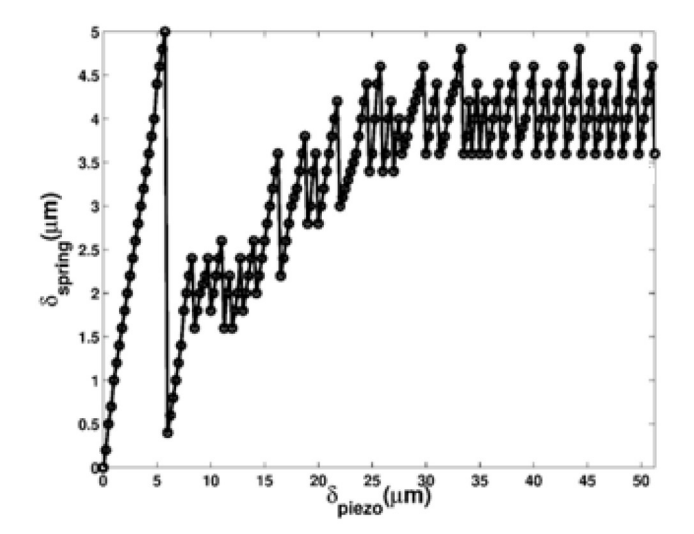


Figure 2. Deflection of the MEMS flexural elements versus the displacement of the piezo stage.

dries, capillary forces produced under the μ cantilever pull the overlapping part of the μ cantilever beam onto the substrate causing a high quality stiction failure.

It is important to note that the critical strain energy release rate is independent of the adhered length, but the force needed to initiate slippage is not. It was observed that the tensile stresses developed inside the μ cantilever can get large enough to break the sample or damage the MEMS sensor if a much longer part of the μ cantilever is stiction failed on the substrate. Thus only 155 μ m of the beam can be failed, without damage to the rest of the setup.

2.2.2. Experimental measurements. To control the growth of the crack and enable measurements of the stiction failed length of the beam using an interferometer, the actuator via the z-axis of the piezo stage is raised by 525 nm. Lifting the actuator creates an s-shaped failure in the μ cantilever beam allowing for direct detection of crack propagation and the deformation profile via the interferometer. A height of 525 nm is selected since it is less than $\frac{1}{4}$ of the thickness of the beam, ensuring a linear mechanical response and it allows for easy detection of crack fronts. The x-axis of the piezo is then indexed by 100 nm increments to 50 μ m. At each step the relative displacement of the MEMS sensor is measured, and the failed length of the beam is determined using the interferometer. The results of the experiment are the relative displacement of the MEMS sensor versus the applied displacement of the piezo, as seen in figure 2.

3. Analysis of experimental results

3.1. Force required to initiate 'slip' events

To convert the MEMS sensor displacements into the force applied the effective stiffness of the system, the stiffness of its beams, must be characterized. Since the system is fabricated from Si, a linear elastic material, each component can be modeled as a combination of springs. The shuttle and μ cantilever specimen are not considered in the analysis because they are approximately 10000 times stiffer than the flexural arms

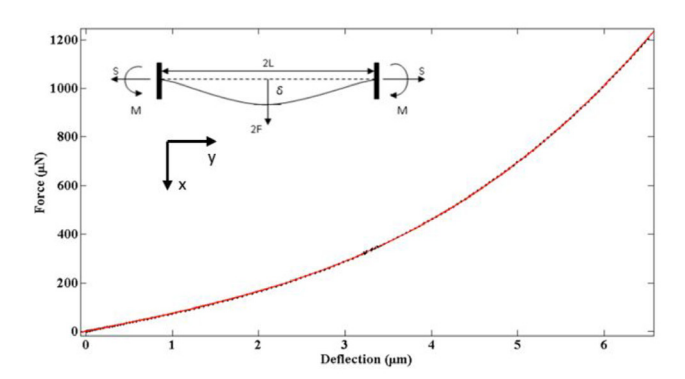


Figure 3. Comparison of Frisch-Fay model for nonlinear fixed-fixed beams and the third order polynomial approximation.

(fixed-fixed beams of figure 1) of the sensor. The flexural arms are modeled using Frisch-Fay's [34] method for large deflections. However, this solution involves iterative simultaneous solution of two coupled nonlinear equations. To simplify this relationship, it is approximated as a third order polynomial. Figure 3 compares the two models in the range of deflections observed in the experiments here. The results of which show that the force in the cantilever is given in equation (1), where $k_1 = 72.17 \text{ N m}^{-1}$ and $k_3 = 2.674 \text{ N m}^{-3}$

$$F(\delta) = k_1 \delta + k_3 \delta^3. \tag{1}$$

Since the device is always in static equilibrium, the external force is always balanced by the reaction force from the springs. The work done by this external force is stored in the MEMS sensor elastically. To calculate the strain energy stored in the system integrate the infinitesimal work of external force, $F(\delta)$, over the shuttle deflection, δ , as shown in equation (2)

$$U = \int_0^{\delta} \left(k_1 \delta + k_3 \delta^3 \right) d\delta = \frac{k_1 \delta^2}{2} + \frac{k_3 \delta^4}{4}.$$
 (2)

Strain energy release rate is conceptually defined as the energy associated with the creation of two new surface areas from a bulk material. This concept is widely used in fracture mechanics to define the critical situation that crack will propagate inside a material. The crack propagation is usually studied in either of two situations: under constant force or constant crack-tip-deflection. The case studied in this paper is the latter. The MEMS sensor is quasi-statically moved away from the substrate to allow a crack to propagate between the μ cantilever and the substrate. As the MEMS sensor is pulled away, the spring system starts to deflect and store energy. This energy was defined mathematically by Griffith [35, 36] as $G = -\frac{\partial U}{\partial A}$, where ∂A represents the new surface area created. For every material there is a critical strain energy release rate that must be reached before a new interface is created. The critical strain energy release rate can be described as in equation (3). Here ∂L_f is the slippage length of the μ cantilever beam over the substrate and w is the width of the beam. L_f is defined as the failed length of the μ cantilever, which is adhered to the substrate and is equal to the total length of the μ cantilever minus the crack length. The crack length is defined as the length of the portion of the μ cantilever which spans between the substrate and the MEMS device. Throughout the

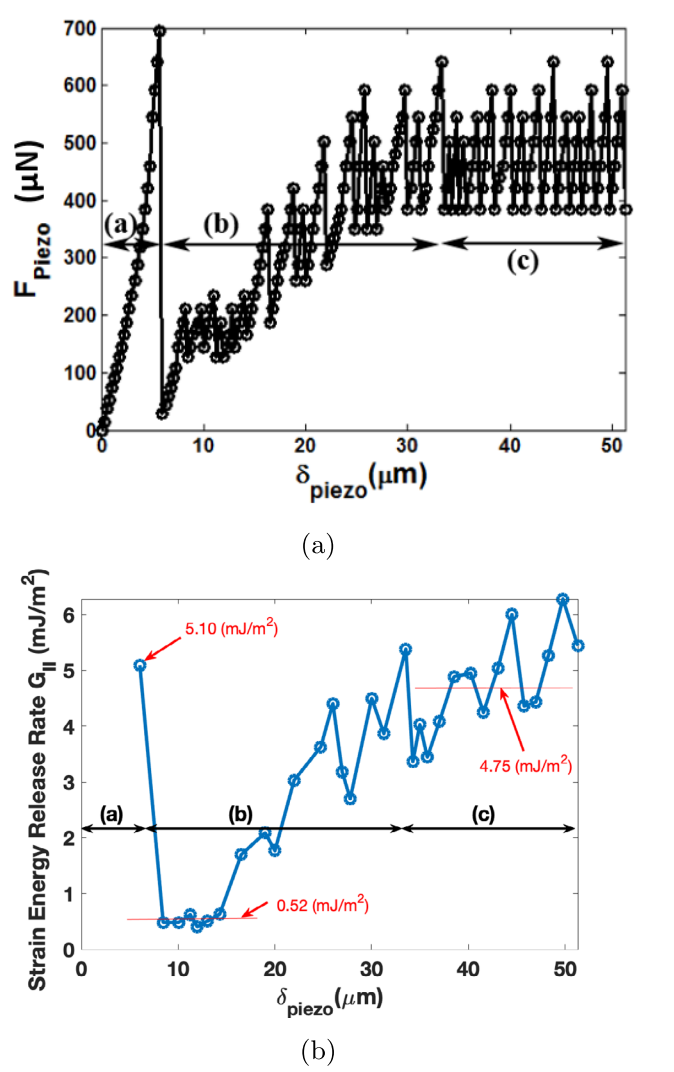


Figure 4. Analysis of experimental results: Force required to initiate slip events (a) and the associated critical strain energy release rate values (b) are plotted as a function of piezo stage displacement.

experiment, L_f increases by each slip event (also called crack arrests) and the crack length increases. The increase in crack arrest is equal to the decrease in L_f , and thus one can use one to determine the other.

$$G_{cr} = -\frac{1}{w} \frac{\partial U}{\partial L_f}.$$
 (3)

The experimental results of figure 2 shows numerous slip-stick events happening due external force applied by the MEMS apparatus and the motion of the piezo stage. Using equation (1) the force applied by the MEMS apparatus can be directly calculated from the experimental data as shown in figure 4(a). Note that following the initial slip event the force does not return to zero. This may be due to secondary bond formation as velocity decreases following the initial slip resulting in re-adhesion of the μ cantilever onto the substrate. It is observed that immediately after the first slip event, the force required to induce subsequent slips reduces drastically but then gradually starts to increase again during the transition region (b) of figure 4(a). After 13 slip-stick cycles, the force

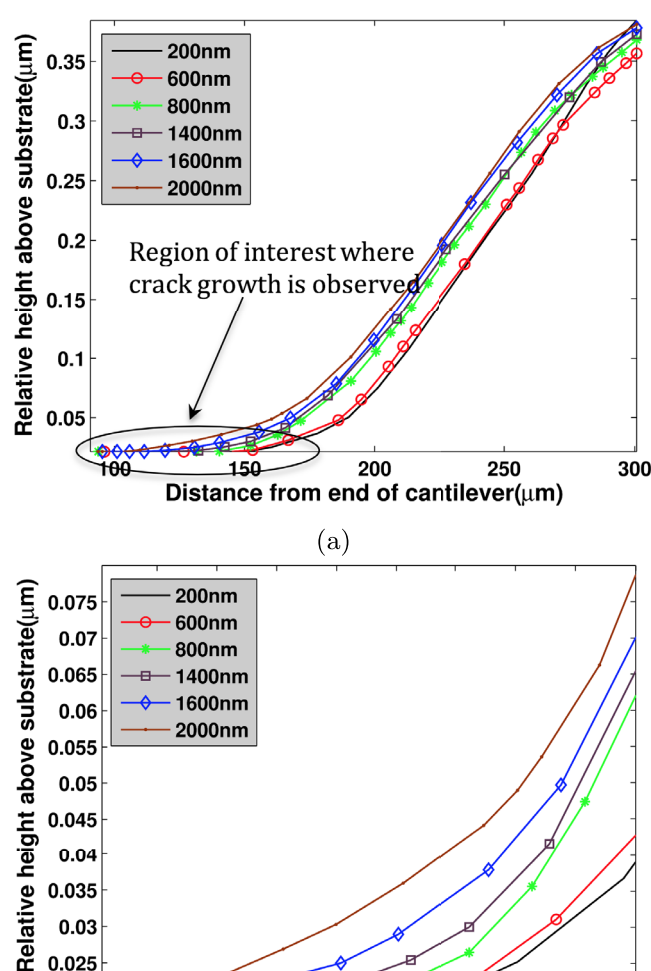


Figure 5. An s-shaped μ cantilever profile is achieved by a small out-of-plane deflection. This allows direct determination of slip events and facilities accurate determination of crack length. The crack tip, marked by ellipse in (a), is magnified in (b).

130

(b)

140

Distance from end of cantilever(µm)

150

120

required to cause further slips stays relatively constant at magnitudes comparable to its initial value.

The authors believe that this observed phenomenon is due to material that is broken away from the surface following each slip event. The large force used to initiate slip, is large enough to break off some of the engaged surface asperities and peaks of the adhered surfaces. The broken pieces of material remain in contact with the two surfaces and can act like ball bearings, rotating to aid in further slippage. These particles also reduce the contact area by creating a gap between the two surfaces [37]. The overall effect is the observed reduction in the required force. The broken particles and debris eventually rest in the valleys between the remaining peaks thereby reducing the overall gap and saturating the effective contact area between the surfaces which finally results in the observed increase in the required force. This effect is confirmed by postmortem surface roughness measurements of the μ cantilever using an atomic force microscopy. It was observed that the average roughness of the μ cantilever increased from 24.9 nm to 64.0 nm.

0.045

0.04 0.035 0.03 0.025

3.2. Determination of accurate values of L_f and G_{II}

As evident from equation (3), in order to determine the critical strain energy release rate (adhesion energy) accurately, it is important to obtain the the values of L_f with high accuracy. To facilitate accurate measurements of L_f , a constant elevation difference—less than $\frac{1}{4}$ of thickness of the μ cantilever—is maintained between the two ends of the μ cantilever specimen. This considerably small out-of-plane deformation results in an overall s-shape (see figure 5) which allows direct measurement of the crack length using the interferometric microscope [25]. It also simplifies detection of slip events. However a closer study of figure 5 reveals that, the small slopes at the crack edge makes accurate determination of crack-tip challenging. In order to overcome this and increase the accuracy even more, a beam model [14] can be employed in conjunction with the interferometric data to determine accurate values of L_f .

After determination of L_f , the data in figure 4(a) are used to calculate the critical strain energy release rate values, shown in figure 4(b). The trends observed in $G_{\rm II}$ values are analogous to those observed in figure 4(a). Although the out of-plane-deflection used in this method is relatively small it does introduce bending and thus some 'Mode I' component. It is crucial to determine the overall contribution of bending in the over-all elastic energy stored in the μ cantilever. It can be shown that the elastic energy stored due to bending is only 0.028% of that due to tensile loading, thus this value of $G_{\rm II}$ is only due to tensile loading.

4. Conclusion

This work presents a novel technique to determine the Mode II critical strain energy release rate. Separate new theories and experiments are developed to determine a $G_{\rm II}$ value accurately. The initial critical strain energy release rate was determined to be $G_{\rm II} = 5.10$ mJ m $^{-2}$. It was observed that $G_{\rm II}$ value decreases considerably after the first slip-event but it gradually climbs back up to the initial range over multiple subsequent stickslips event. During the first half of the transition region the $G_{\rm II}$ values, initially decrease to an average of 0.520 mJ m $^{-2}$ but then start to gradually increase in the second half of transition region. After multiple stick-slip events the $G_{\rm II}$ values stabilize at an average value of 4.75 mJ m $^{-2}$. This values are in line with earlier experiments by the authors that included mixed mode (Modes I and II) effects [14, 15]

As the surface roughness plays an important role in the adhesion of MEMS structures, the surfaces that were involved in the experiments are characterized with atomic force microscopy. It is observed that the surface roughness of an experimentally rubbed surface of μ cantilever beam has more RMS roughness compared to a virgin lower surface of μ cantilever beam. These values are 64.0 nm and 24.9 nm, respectively. From the characterization of surface of the μ cantilever, it is hypothesized that local peaks of poly-Si broke and came to rest in the valleys between other local peaks of

 μ cantilever and corresponding surface causing an increased RMS roughness.

Acknowledgments

The authors acknowledge support from the National Science Foundation (NSF CMMI-1662879). Portions of the work were carried out in UNM's Manufacturing Training and Technology Center and UNM's Nano Synthesis Facility.

ORCID iDs

Arash Kheyraddini Mousavi https://orcid.org/0000-0002-7457-1047

Tyler Jordan Hieber https://orcid.org/0000-0001-5512-5167 James Chen https://orcid.org/0000-0002-5530-6029 Zayd Chad Leseman https://orcid.org/0000-0002-9846-7164

References

- [1] Czaplewski D A, Patrizi G A, Kraus G M, Wendt J R, Nordquist C D, Wolfley S L, Baker M S and de Boer M P 2009 A nanomechanical switch for integration with CMOS logic J. Micromech. Microeng. 19 085003
- [2] Parizi K B, Peyvast N, Mousavi B K, Mohajerzadeh S and Fathipour M 2010 Schottky barrier nano-MOSFET with an asymmetrically oxidized source/drain structure *Solid-State Electron.* 54 48–51
- [3] Karbassian F, Mousavi B K, Rajabali S, Talei R, Mohajerzadeh S and Asl-Soleimani E 2014 Formation of luminescent silicon nanowires and porous silicon by metalassisted electroless etching *J. Electron. Mater.* 43 1271–9
- [4] Kheyraddini Mousavi B 2018 Selected applications of silicon nanopillar arrays *PhD Thesis* The University of New Mexico
- [5] Bernstein J et al 2003 An overview of MEMS inertial sensing technology Sensors: J. Appl. Sensing Technol. 20 14–21
- [6] Alaie S, Goettler D F, Su M, Leseman Z C, Reinke C M and El-Kady I 2015 Thermal transport in phononic crystals and the observation of coherent phonon scattering at room temperature *Nat. Commun.* 6 7228
- [7] Abbas K 2009 Design fabrication and calibration of MEMS actuators for *in situ* materials testing *PhD Thesis* The University of New Mexico
- [8] Mousavi A K, Atwater M A, Mousavi B K, Jalalpour M, Taha M R and Leseman Z C 2014 Mechanical and electrical characterization of entangled networks of carbon nanofibers *Materials* 7 4845–53
- [9] Alaie S, Mousavi A K, Su M and Leseman Z C 2010 Finite element analysis of a phononic crystal at gigahertz frequencies ASME 2010 Int. Mechanical Engineering Congress and Exposition (American Society of Mechanical Engineers) pp 389–93
- [10] Hornbeck L J 2001 The dmd tm projection display chip: a MEMS-based technology MRS Bull. 26 325–7
- [11] Romig A D and McWhorter P J 2001 Intelligent micromachines: opportunities and challenges of the next si revolution *Semicon*, *Europe*
- [12] Romig A D and McWhorter P J 2001 Opportunities and challenges in MEMS commercialization Vac. Technol. Coat.
- [13] O'neill J F, Drake D J and Hawkins W G 1989 Method of fabricating ink jet printheads US Patent 4,875,968

- [14] Mousavi A K, Kashamolla M R and Leseman Z C 2013 Improved model for the adhesion of μcantilevers: theory and experiments J. Micromech. Microeng. 23 115011
- [15] Kheyraddini Mousavi A 2015 Characterization of mechanical properties at the micro/nano scale: stiction failure of MEMS, high-frequency Michelson interferometry and carbon nanoFibers *PhD Thesis* The University of New Mexico
- [16] Kashamolla M R, Goettler D F, Mousavi A K and Leseman Z C 2010 Mode II measurements for stiction failed MEMS devices ASME 2010 Int. Mechanical Engineering Congress and Exposition (American Society of Mechanical Engineers) pp 63–9
- [17] Kheyraddini Mousavi A, Alaie S and Leseman Z C 2016 Basic MEMS actuators *Encyclopedia of Nanotechnology* (Netherlands: Springer) pp 1–16
- [18] Srinivasan U, Foster J D, Habib U, Howe R T, Maboudian R, Senft D C and Dugger M T 1998 Lubrication of polysilicon micromechanisms with self-assembled monolayers *Technical Report* Sandia National Labs. SAND-98-0848C
- [19] Ma J Q, Pang C J, Mo Y F and Bai M W 2007 Preparation and tribological properties of multiply-alkylated cyclopentane (MAC)—octadecyltrichlorosilane (OTS) double-layer film on silicon Wear 263 1000-7
- [20] Alley R L, Howe R T and Komyopoulos K 1995 Method of applying a monolayer lubricant to micromachines US Patent 5,403,665
- [21] Maboudian R, Ashurst W R and Carraro C 2002 Tribological challenges in micromechanical systems *Tribol. Lett.* 12 95–100
- [22] Chen D and Xiong F 2008 Method of using a preferentially deposited lubricant to prevent anti-stiction in micromechanical systems US Patent 7,463,404
- [23] Corwin A D, Street M D, Carpick R W, Ashurst W R, Starr M J and De Boer M P 2006 Friction of different monolayer lubricants in MEMS interfaces Sandia Report Sandia National Laboratories SAND2005-7954
- [24] Carpick R W, Street M D, Ashurst W R and Corwin A D 2006 Friction of different monolayer lubricants in MEMS

- interfaces *Technical Report* Sandia National Laboratories SAND2005-7954
- [25] de Boer M P and Michalske T A 1997 Accurate method for determining adhesion of cantilever beams J. Appl. Phys. 86 817–27
- [26] Strus M C, Zalamea L, Raman A, Pipes R B, Nguyen C V and Stach E A 2008 Peeling force spectroscopy: exposing the adhesive nanomechanics of one-dimensional nanostructures *Nano Lett.* 8 544–50
- [27] Gorthi S, Mohanty A and Chatterjee A 2006 Cantilever beam electrostatic MEMS actuators beyond pull-in *J. Micromech. Microeng.* 16 1800–10
- [28] Jones E E, Begley M R and Murphya K D 2003 Adhesion of micro-cantilevers subjected to mechanical point loading: modeling and experiments J. Mech. Phys. Solids 51 1601–22
- [29] Leseman Z C, Carlson S P and Mackin T J 2007 Experimental measurements of the strain energy release rate for stictionfailed microcantilevers using a single-cantilever beam peel test J. Microelectromech. Syst. 16 38–43
- [30] Leseman Z C 2006 A novel method for testing freestanding nanofilms using a custom MEMS load cell *PhD Thesis* University of Illinois at Urbana-Champaign
- [31] Laermer F and Schilp A 1996 Method of anisotropically etching silicon *US Patent* 5,501,893
- [32] Jorgensen C R and Yarberry V R 2001 A 3D geometry modeler for the SUMMiT V MEMS designer *Modeling and Simulation of Microsystems* pp 594–7
- [33] Sniegowski J J and De Boer M P 2000 IC-compatible polysilicon surface micromachining Ann. Rev. Mater. Sci. 30 299–333
- [34] Frisch-Fay R 1962 Flexible Bars (London: Butterworths)
- [35] Edwalds H L and Wanhill R J H 1984 Fracture mechanics (London, Edward Arnold)
- [36] Lawn B and Wilshaw T R 1993 Fracture of Brittle Solids (Cambridge: Cambridge University Press)
- [37] Yapu Z 2003 Stiction and anti-stiction in MEMS and NEMS Acta Mech. Sin. 19 1–10